Fluorescence molecular-tomography reconstruction with *a priori* anatomical information

Lu Zhou[a], Birsen Yazici[a], Vasilis Ntziachristos[b]

[a]Rensselaer Polytechnic Institute, 110 8th Street, Troy, NY, USA;
[b]Harvard Medical School, 25 Shattuck Street, Boston, MA, USA

ABSTRACT

In this study, we combine a generalized Tikhonov regularization method with *a priori* anatomical information to reconstruct the concentration of fluorophores in mouse with Chronic Obstructive Pulmonary disease (COPD) from *in vivo* optical and Magnetic Resonance (MR) measurements. Generalized Tikhonov regularization incorporates a penalty term in the optimization formulation of the fluorescence molecular tomography (FMT) inverse problem. Our design involves two penalty terms to make use of *a priori* anatomical structural information from segmented MR images. The choice of the penalty terms guide the fluorophores in reconstructed image concentrates in the region where it is supposed to be and assure smooth flourophore distribution within tissue of same type and enhances the discontinuities between different tissue types. We compare our results with traditional Tikhanov regularization techniques in extensive simulations and demonstrate the performance our approach *in vivo* mouse data. The results show that the increased fluorophore concentration in the mouse lungs is consistent with an increased inflammatory response expected from the corresponding animal disease model.

Keywords: *a priori* information, fluorescence molecular tomography (FMT), Tikhonov regularization

1. INTRODUCTION

Fluorescence molecular tomography (FMT) is a technology directed towards noninvasive quantitative molecular imaging of whole animals and tissues.[1]It offers fully three-dimensional functional images to explore the fluorophore activity inside biological tissue. FMT is an ill-posed inverse problem which presents certain challenges. It suffers from a large number of unknowns and a relatively limited number of measurements which essentially causes the under-determination property. In mean time, the solution of the FMT inverse problem is also highly sensitive to the noise in the measurements. Therefore, regularization is needed in the reconstruction to obtain a stable solution. Tikhonov regularization is a widely-used technique to deal with the ill-posedness of the inverse problem. Based on the assumption that the magnitude of solution is small and varies slowly within the support, the Tikhonov regularization method formulates the inverse problem into an optimization framework and constrains the magnitude and gradient of the solution by introducing penalty terms in objective functional of optimization. The traditional Tikhonov regularization method provides us with a way to acquire a stable solution, but the resolution and contrast of the reconstructed image are still very low. A promising way to improve the reconstruction result is by using *a priori* information provided by another anatomical imaging modalities such as Magnetic Resonance Imaging (MRI) and X-ray to guide the reconstruction process. The effectiveness of incorporating prior information in FMT reconstruction has been proved in several recent studies[2].[3]

For diffuse optical tomography (DOT), a number of approaches have incorporated *a priori* information into reconstruction[45].[6] Unlike the DOT problem where the average optical absorption coefficient and scattering coefficient are known, it is not possible to obtain an average fluorophore concentration value for the FMT problem nor to use such information to guide reconstruction. In the FMT problem, typically two types of prior information are available. One is the localization information of a certain fluorophore type based on its chemical and physical properties. The other is the internal edge structure information of an optical medium from another anatomical imaging modality.[7] For example, the fluorophore may target certain organs, and in the anatomical images such as MR and X-ray images, these organs can be well segmented and located. In this case, the penalty term in generalized Tikhonov regularization method can be designed to constrain the location of fluorophore

Send correspondence to Birsen Yazici: E-mail: yazici@ecse.rpi.edu

Small Animal Whole-Body Optical Imaging Based on Genetically Engineered Probes
edited by Alexander P. Savitsky, Robert E. Campbell, Robert M. Hoffman
Proc. of SPIE Vol. 6868, 68680O, (2008) · 1605-7422/08/$18 · doi: 10.1117/12.763269

concentration within these organs. On the other hand, the edge information in the anatomical images can also be used to constrain the spatial variation and smoothness of the solution.

In this work, we formulate the inverse problem of FMT into an optimization framework with a generalized Tikhonov regularization method. We use *a priori* information about the localization of the fluorophore concentration and anatomical structural information of the imaging domain to formulate the penalty terms in generalized Tikhonov regularization. In the simulation study and the *in vivo* mouse experiment, we reconstruct the FMT images with and without the incorporation of prior information and suggest a method to choose optimal regularization parameters. The improved reconstruction result indicates the advantage and effectiveness of our method of using *a priori* anatomical information in FMT reconstruction. In addition, we also reconstruct the images using prior information inconsistent with true fluorophore distribution in simulation, results show us the insensitivity of our method to wrong prior information.

The outline of this paper is as follow: Section 2 gives a brief introduction about the forward and inverse problems of FMT. In Section 3, we discuss how to incorporate available *a priori* anatomical information into generalized Tikhonov regularization and discretization of the objective functional. In Section 4 and 5, we perform simulations and an *in vivo* mouse experiment and present improved reconstruction results by incorporating *a priori* anatomical information into the reconstruction.

2. FORWARD AND INVERSE PROBLEM OF FMT

2.1 The Forward Problem

In frequency domain, the propagation of light at the excitation wavelength λ_1 in a bounded domain $\Omega \subset \mathbb{R}^3$ can be described by the diffusion equation below with a Robin boundary condition:[8]

$$-\nabla \cdot D^{\lambda_1}(\mathbf{x})\nabla\Phi_j^{\lambda_1}(\mathbf{x}) + [\mu_a^{\lambda_1}(\mathbf{x}) + \frac{i\omega}{c}]\Phi_j^{\lambda_1}(\mathbf{x}) = Q_j(\mathbf{x}), \quad \mathbf{x} \in \Omega, \tag{1}$$

$$\Phi_j^{\lambda_1}(\mathbf{x}) + 2aD^{\lambda_1}(\mathbf{x})\frac{\partial\Phi_j^{\lambda_1}(\mathbf{x})}{\partial n} = 0, \quad \mathbf{x} \in \partial\Omega, \tag{2}$$

where $\Phi_j^{\lambda_1}(\mathbf{x})$ is the isotropic photon density at excitation wavelength λ_1 due to the jth source $Q_j(\mathbf{x})$. $Q_j(\mathbf{x})$ is the point source at $\mathbf{x}_s^j$, $D^{\lambda_1}(\mathbf{x})$ and $\mu_a^{\lambda_1}(\mathbf{x})$ are the diffusion coefficient and absorption coefficient to the light with wavelength λ_1. ω is the modulation angular frequency and c is the speed of light propagating in the medium. n is the direction perpendicular to the boundary, and a is the boundary mismatch parameter due to the light reflection on the boundary.

For emission light at wavelength λ_2, the photon density is described as below:[9]

$$-\nabla \cdot D^{\lambda_2}(\mathbf{x})\nabla\Phi_j^{\lambda_2}(\mathbf{x}) + [\mu_a^{\lambda_2}(\mathbf{x}) + \frac{i\omega}{c}]\Phi_j^{\lambda_2}(\mathbf{x}) = \Phi_j^{\lambda_1}(\mathbf{x})\eta\mu_{af}(\mathbf{x})\frac{1 - i\omega\tau(\mathbf{x})}{1 + [\omega\tau(\mathbf{x})]^2}, \quad \mathbf{x} \in \Omega, \tag{3}$$

$$\Phi_j^{\lambda_2}(\mathbf{x}) + 2aD^{\lambda_2}(\mathbf{x})\frac{\partial\Phi_j^{\lambda_2}(\mathbf{x})}{\partial n} = 0, \quad \mathbf{x} \in \partial\Omega, \tag{4}$$

where $\mu_{af}(\mathbf{x})$ is the absorption coefficient due to fluorophore and $\tau(\mathbf{x})$ is the fluorescence lifetime. η is quantum yield and is defined as the ratio of the number of photons emitted to the number of photons absorbed.

2.2 The Inverse Problem

The inverse problem of FMT consists of finding the unknown fluorophore concentration from measurements on the boundary. First, we state the adjoint problem[8] associated with equation (1) and (2), but at wavelength λ_2:

$$-\nabla \cdot D^{\lambda_2}(\mathbf{x})\nabla\Psi_k^{\lambda_2}(\mathbf{x}) + [\mu_a^{\lambda_2}(\mathbf{x}) - \frac{i\omega}{c}]\Psi_k^{\lambda_2}(\mathbf{x}) = 0, \quad \mathbf{x} \in \Omega, \tag{5}$$

$$\Psi_k^{\lambda_2}(\mathbf{x}) + 2aD^{\lambda_2}(\mathbf{x})\frac{\partial\Psi_k^{\lambda_2}(\mathbf{x})}{\partial n} = Q_k^*(\mathbf{x}), \quad \mathbf{x} \in \partial\Omega, \tag{6}$$

where $\Psi_k^{\lambda_2}(\mathbf{x})$ is the photon density of the adjoint problem, $Q_k^*(\mathbf{x})$ is the adjoint source located at kth detector's position $\mathbf{x}_d^k$.

Assume the Green's function to equation(5) and (6) is given by $G_k^{\lambda_2}(\mathbf{x})$, then the relationship between the measurements of kth detector at $\mathbf{x}_d^k$ due to jth source at $\mathbf{x}_s^j$ and the fluorophore concentration is

$$\Gamma_{k,j} = \int_\Omega G_k^{\lambda_2}(\mathbf{x})\Phi_j^{\lambda_1}(\mathbf{x})\eta\mu_{af}(\mathbf{x})\frac{1-i\omega\tau(\mathbf{x})}{1+[\omega\tau(\mathbf{x})]^2}d\mathbf{x}. \tag{7}$$

If there are N_s sources and N_d detectors, the total number of measurements is $M = N_s \times N_d$. The measurements $\Gamma_{k,j}$ can be assembled into an $M \times 1$ vector $\Gamma = [\Gamma_{1,1}, \Gamma_{2,1}, \ldots, \Gamma_{N_d,1}, \Gamma_{1,2}, \Gamma_{2,2}, \ldots, \Gamma_{N_d,N_s}]^T$. If the amplitude of the source is time invariant, known as continuous wave (CW) FMT, then equation (7) can be simplified as:[7]

$$\begin{aligned}\Gamma_{(j-1)\times N_s+k} &= \int_\Omega G_k^{\lambda_2}(\mathbf{x})\Phi_j^{\lambda_1}(\mathbf{x})\alpha(\mathbf{x})d\mathbf{x}, \\ &= \int_\Omega H_{(j-1)\times N_s+k}(\mathbf{x})\alpha(\mathbf{x})d\mathbf{x}, \\ &= \mathcal{A}_f(\alpha(\mathbf{x}))\end{aligned} \tag{8}$$

where $\alpha(\mathbf{x}) = \eta\mu_{af}(\mathbf{x})$ can be considered the fluorophore concentration. $H_{(j-1)\times N_s+k}(\mathbf{x}) = G_k^{\lambda_2}(\mathbf{x})\Phi_j^{\lambda_1}(\mathbf{x})$ is the $((j-1)\times N_s + k)$th kernel of the linear vector-valued operator $\mathcal{A}_f : H^1(\Omega) \to \mathbb{R}^{M\times 1}$.

If we apply the adjoint operator of $\mathcal{A}_f$ to both side of equation (8), and let $\mathcal{A} = \mathcal{A}_f^*\mathcal{A}_f : H^1(\Omega) \to H^1(\Omega)$, $\gamma = \mathcal{A}_f^*\Gamma \in H^1(\Omega)$, then we have the forward model:[7]

$$\gamma(\mathbf{x}) = \mathcal{A}(\alpha(\mathbf{x})). \tag{9}$$

This equation connects the measurements at boundary to the fluorophore concentration, where the operator $\mathcal{A}$ is the forward operator. The inverse problem is solving this equation for $\alpha(\mathbf{x})$ by knowing $\gamma(\mathbf{x})$ and $\mathcal{A}$.

3. INCORPORATION OF THE *A PRIORI* ANATOMICAL INFORMATION INTO GENERALIZED TIKHONOV REGULARIZATION

3.1 Theory

The generalized Tikhonov regularization minimizes the objective functional

$$\mathcal{F}(\alpha(\mathbf{x})) = \int_\Omega |\gamma(\mathbf{x}) - \mathcal{A}(\alpha(\mathbf{x}))|^2 d\mathbf{x} + \delta\hat{\mathcal{G}}(\alpha(\mathbf{x})), \tag{10}$$

to solve the inverse problem $\gamma(\mathbf{x}) = \mathcal{A}(\alpha(\mathbf{x}))$, where $\hat{\mathcal{G}} : H^1(\Omega) \to \mathbb{R}$ is a nonnegative penalty functional and δ is a regularization parameter. A common choice for $\hat{\mathcal{G}}$ is a functional of the form

$$\hat{\mathcal{G}}(\alpha(\mathbf{x})) = \int_\Omega |\mathcal{L}(\alpha(\mathbf{x}) - \hat{\alpha}(\mathbf{x}))| d\mathbf{x}, \tag{11}$$

where $\mathcal{L} : H^1(\Omega) \to H^1(\Omega)$ is an appropriately chosen regularizing operator and $\hat{\alpha}(\mathbf{x})$ is a prior estimate of $\alpha(\mathbf{x})$.

In FMT problem, it is difficult to obtain the exact estimation $\hat{\alpha}(\mathbf{x})$ about the magnitude of solution $\alpha(\mathbf{x})$. Based on the anatomical images from MRI, X-ray or other medical imaging modalities, different types of tissue and organs can be well classified and located. One type of prior information is the localization information of fluorophore concentration. Another type of prior information is the internal edge structure information of imaging domain. That is, the spatial distribution of fluorophore concentration is expected to be discontinuous across the boundary of different tissue and organs.

The first type of information can be incorporated into Tikhonov regularization by using the regularizing operator introduced by Arridge.[10] Equation (11) takes the form of a penalty term $\mathcal{R}(\alpha(\mathbf{x}))$:

$$\mathcal{R}(\alpha(\mathbf{x})) = \int_\Omega |r(\mathbf{x})\alpha(\mathbf{x})|^2 d\mathbf{x}, \tag{12}$$

where $r(\mathbf{x})$ is a positive function with a lower value at positions where the fluorophore is expected to be. Therefore, the penalty is weaker in regions where fluorophore is likely to be present.

For the second type of information, we can use the regularizing operator introduced by Kaipio,[11] and formulate the penalty term $\mathcal{B}(\alpha(\mathbf{x}))$:

$$\mathcal{B}(\alpha(\mathbf{x})) = \int_\Omega \|\tilde{B}(\mathbf{x})\nabla\alpha(\mathbf{x})\|^2 d\mathbf{x}, \tag{13}$$

where $\tilde{B} : \Omega \to \mathbb{R}^{3\times 3}$ is a matrix-valued mapping on Ω. If the structural information is given in the form of a function $s(\mathbf{x})$, then $\tilde{B}$ can be defined as

$$\tilde{B}(\mathbf{x}) = I - (1 + \|\nabla s(\mathbf{x})\|^2)^{-1}\nabla s(\mathbf{x})(\nabla s(\mathbf{x}))^T, \tag{14}$$

where the eigenvalues of $\tilde{B}(\mathbf{x})$ are $\lambda_1(\mathbf{x}) = \lambda_2(\mathbf{x}) = 1$ and $\lambda_3(\mathbf{x}) = (1+\|\nabla s(\mathbf{x})\|^2)^{-1}$. The eigenvector corresponding to λ_3 is $v_3(\mathbf{x}) = \|\nabla s(\mathbf{x})\|^{-1}\nabla s(\mathbf{x})$ $(\nabla s(\mathbf{x}) \neq 0)$. By using eigenvalue decomposition of $\tilde{B}(\mathbf{x})$, equation(13) becomes

$$\mathcal{B}(\alpha(\mathbf{x})) = \sum_{j=1}^{3} \int_\Omega |\lambda_j(\mathbf{x}) v_j^T(\mathbf{x}) \cdot \nabla\alpha(\mathbf{x})|^2 d\mathbf{x}. \tag{15}$$

This functional is the square integral norm of the derivative of $\alpha(\mathbf{x})$ in direction of $\tilde{B}(\mathbf{x})$'s eigenvectors v_j with weights λ_j. Notice that the last eigenvector is the normalized $\nabla s(\mathbf{x})$ and the eigenvalue for this eigenvector is small when $\|\nabla s(\mathbf{x})\|$ is large. Therefore, given a point close to a discontinuity in prior structural image $s(\mathbf{x})$ (i.e. the boundary between different tissue), the penalty for a rapid change of $\alpha(\mathbf{x})$ when $\mathbf{x}$ moves towards the discontinuity (i.e. along the direction of $\nabla s(\mathbf{x})$) is smaller compared to the penalty when $\mathbf{x}$ moves along the discontinuity[11](i.e. along the directions of other eigenvectors). If $\nabla s(\mathbf{x}) = 0$, $\tilde{B}(\mathbf{x}) = I$, the penalty for a change of $\alpha(\mathbf{x})$ in all directions is the same for $\mathbf{x}$ moves along the discontinuity. This forces the reconstructed image to be smooth except at the boundary of different tissues, where the image can show large changes.

Then, equation(10) is expressed as

$$\mathcal{F}(\alpha(\mathbf{x})) = \int_\Omega |\gamma(\mathbf{x}) - \mathcal{A}(\alpha(\mathbf{x}))|^2 d\mathbf{x} + \delta_1\mathcal{R}(\alpha(\mathbf{x})) + \delta_2\mathcal{B}(\alpha(\mathbf{x})). \tag{16}$$

δ_1 and δ_2 are regularization parameters which balance the weights of two penalty terms and data residual $\|\gamma(\mathbf{x}) - \mathcal{A}(\alpha(\mathbf{x}))\|$.

3.2 Discretization

We discretize $\Omega \subset \mathbb{R}^3$ into N voxels, then use $\alpha = [\alpha^{(1)}, \ldots, \alpha^{(N)}]^T$ to denote reconstructed image. Here, we consider a simple case of prior structural information. Suppose Ω is divided into two region S and Ω/S, we know the fluorophore is only in region S. Let $s = [s^{(1)}, \ldots, s^{(N)}]^T$ present the discretized prior structural image $s(\mathbf{x})$,

$$s^{(i)} = \begin{cases} s_0 & \text{if the } i\text{th voxel} \in S, \\ 0 & \text{if the } i\text{th voxel} \in \Omega/S. \end{cases} \tag{17}$$

The partial derivatives $\partial s/\partial x_k, k = 1, 2, 3$ in $\nabla s(\mathbf{x})$ are computed using finite difference approximation as $D_k s$, where D_k is difference operator matrix in this type:

$$D_k = \begin{pmatrix} -1 & 0 & \cdots & 0 & 1 & 0 & 0 & \cdots \\ 0 & -1 & 0 & \cdots & 0 & 1 & 0 & \cdots \\ 0 & 0 & -1 & 0 & \cdots & 0 & 1 & \cdots \\ \vdots & & & \ddots & & & & \ddots \end{pmatrix}_{N\times N}.$$

$\tilde{B}(\mathbf{x})$ and its eigenvalues $\lambda_j^{(i)}$ and eigenvectors $\mathbf{v}_j^{(i)} = [v_{j1}^{(i)}, v_{j2}^{(i)}, v_{j3}^{(i)}]^T$ $(j = 1, 2, 3)$ at each voxel are computed. We assemble those eigenvalues and eigenvectors as

$$V_{jk} = \begin{bmatrix} v_{jk}^{(1)} & & \\ & \ddots & \\ & & v_{jk}^{(N)} \end{bmatrix}, \qquad \Lambda_j = \begin{bmatrix} \lambda_j^{(1)} & & \\ & \ddots & \\ & & \lambda_j^{(N)} \end{bmatrix}, \qquad j = 1, 2, 3,\ k = 1, 2, 3.$$

Then, the penalty term $\mathcal{B}(\alpha(\mathbf{x}))$ could be discretized as

$$B(\alpha) = \sum_{j=1}^{3} \|\Lambda_j \sum_{k=1}^{3} V_{jk} D_k \alpha\|^2. \tag{18}$$

In this case, we have

$$\lambda_j^{(i)} = \begin{cases} 1/(1+s_0^2) & j = 3 \text{ and } i\text{th voxel is on the boundary between } S \text{ and } \Omega/S, \\ 1 & \text{otherwise.} \end{cases}$$

Notice that the absolute value of s_0 is not necessary to compute V_{jk}. It is only needed to determine the last eigenvalue of $\tilde{B}(\mathbf{x})$. This eigenvalue controls the ratio between the penalty on the change of $\alpha(\mathbf{x})$ when $\mathbf{x}$ moves towards discontinuity and moves along discontinuity. Therefore, we can assume $\lambda_3^{(i)} = \lambda_0$ $(0 < \lambda_0 < 1)$ and choose λ_0 directly to control this ratio.

Similarly, the penalty term $\mathcal{R}(\alpha(\mathbf{x}))$ in equation(16) becomes

$$R(\alpha) = \|R\alpha\|^2, \tag{19}$$

where R is diagonal matrix and

$$r_{m,n} = \begin{cases} r_0 & m = n = i \text{ and } i\text{th voxel} \in S, \\ 1 & m = n = i \text{ and } i\text{th voxel} \in \Omega/S, \\ 0 & m \neq n, \end{cases}$$

and $0 < r_0 < 1$.

We can discretize the operator $\mathcal{A}_f$ into a $M \times N$ matrix A_f, then discretize $\mathcal{A}$ as $A = A_f^H A_f{}^*$ and γ as $\gamma = A_f^H \Gamma$. In the end, we represent the generalized Tikhonov regularization objective functional in matrix form

$$F = \|A\alpha - \gamma\|^2 + \delta_1 \|R\alpha\|^2 + \delta_2 \sum_{j=1}^{3} \|\Lambda_j \sum_{k=1}^{3} V_{jk} D_k \alpha\|^2. \tag{20}$$

4. SIMULATION EXPERIMENT

4.1 Simulation Configuration

The simulation experiment was performed to study the effect of incorporating the prior information into generalized Tikhonov regularization in FMT. We simulated the imaging process of a $5 \times 5 \times 3$ cm slab phantom with interior fluorophore concentration. It was meshed into $10 \times 10 \times 7 = 700$ voxels. The optical properties for this simulation phantom were $\mu_a = 0.05$ cm^{-1} and $\mu_s' = 8$ cm^{-1} $(D = 1/3(\mu_a + \mu_s'))$ for both excitation and emission. Within the phantom, $c = 2 \times 10^8$ m/s, and on the boundary of phantom, $a = 0.5$. A spherical fluorophore with a radius of 1 cm and $\eta\mu_{af} = 0.5$ cm^{-1} was positioned in the center of phantom(see Fig.1(a)). Twenty five unmodulated sources $(\omega = 0)$ and 25 detectors were positioned on 5×5 grids on the top and bottom

* A_f^H is the conjugate transpose of A_f

of phantom respectively. Next, 10% Gaussian white noise was added to the simulated measurements to simulate real FMT imaging.

For the prior information in this simulation, we assumed the exact region of fluorophore given above is known. Therefore, in prior structural image, voxels have value 1 in the central spherical region and 0 outside. Next, we assembled matrices R, Λ_j and V_{jk} described in Section 3.2. In this study, we assumed $R(\alpha)$ and $B(\alpha)$ have same weights in equation(20), therefore we fixed the ratio between δ_1 and δ_2 roughly as $\|R^T R\|_1 / \sum_{j=1}^{3} \|(\Lambda_j \sum_{k=1}^{3} V_{jk} D_k)^T (\Lambda_j \sum_{k=1}^{3} V_{jk} D_k)\|_1$. This makes the value of these two terms roughly the same in scale. Different weights can be chosen on penalty terms $R(\alpha)$ and $B(\alpha)$, if needed.

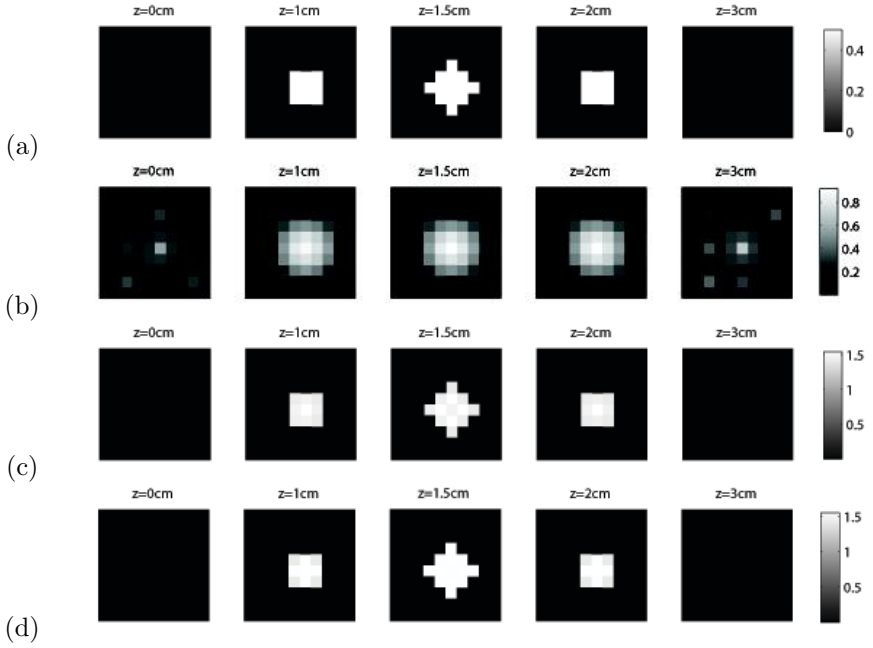

Figure 1. (a) The true image of fluorophore distribution; (b) Reconstructed image without prior information, $\delta_1 = 4 \times 10^{-10}$ and $\delta_2 = 8 \times 10^{-11}$; (c) Reconstructed image with prior information, $\delta_1 = 2 \times 10^{-8}$, $\delta_2 = 4 \times 10^{-9}$ and $\lambda_0 = r_0 = 0.1$; (d) Reconstructed image with prior information, $\delta_1 = 1.5 \times 10^{-6}$, $\delta_2 = 3 \times 10^{-7}$ and $\lambda_0 = r_0 = 0.01$

4.2 Simulation Results

In the first simulation, the image was reconstructed without prior information. We set $r_0 = 1$ and $\lambda_0 = 1$, so traditional 0th and 1st order Tikhonov regularization were combined together during the reconstruction. The L-curve method[12] was used to determine δ_1 and δ_2. The L-curve is the curve between data residual $\|A\alpha - \gamma\|$ and norm of reconstructed image $\|\alpha\|$. The optimal regularization parameter is chosen at the corner of L-shaped curve in Fig.2(a). The direction of increasing δ_0 and δ_1 is indicated by an arrow in this figure. The turning point of this curve is where $\|\alpha\|$ begins to increase faster than $\|A\alpha - \gamma\|$ decreases and the reconstruction begins to fit the noise but not the data. The reconstructed result with optimal parameters is shown in Fig.1(b).

In the second simulation, we made use of prior information in reconstruction. Parameters r_0 and λ_0 are usually chosen empirically. In this simulation, we moderately set $r_0 = 0.1$, $\lambda_0 = 0.1$ and $r_0 = 0.01$, $\lambda_0 = 0.01$. The L-curves for both cases are plotted in Fig.2(b) and (c), and optimal regularization parameters were determined in same way as the first simulation. The final reconstruction results with optimal regularization parameters are shown in Fig.1(c) and (d). We can see a significant improvement of the contrast and resolution in final image.

4.3 Reconstruction Evaluation

To evaluate the result quantitively, we first define some image quality measures for the reconstructed image. The contrast-to-background noise ratio (CBNR) is defined as the ratio of the mean value of the reconstructed

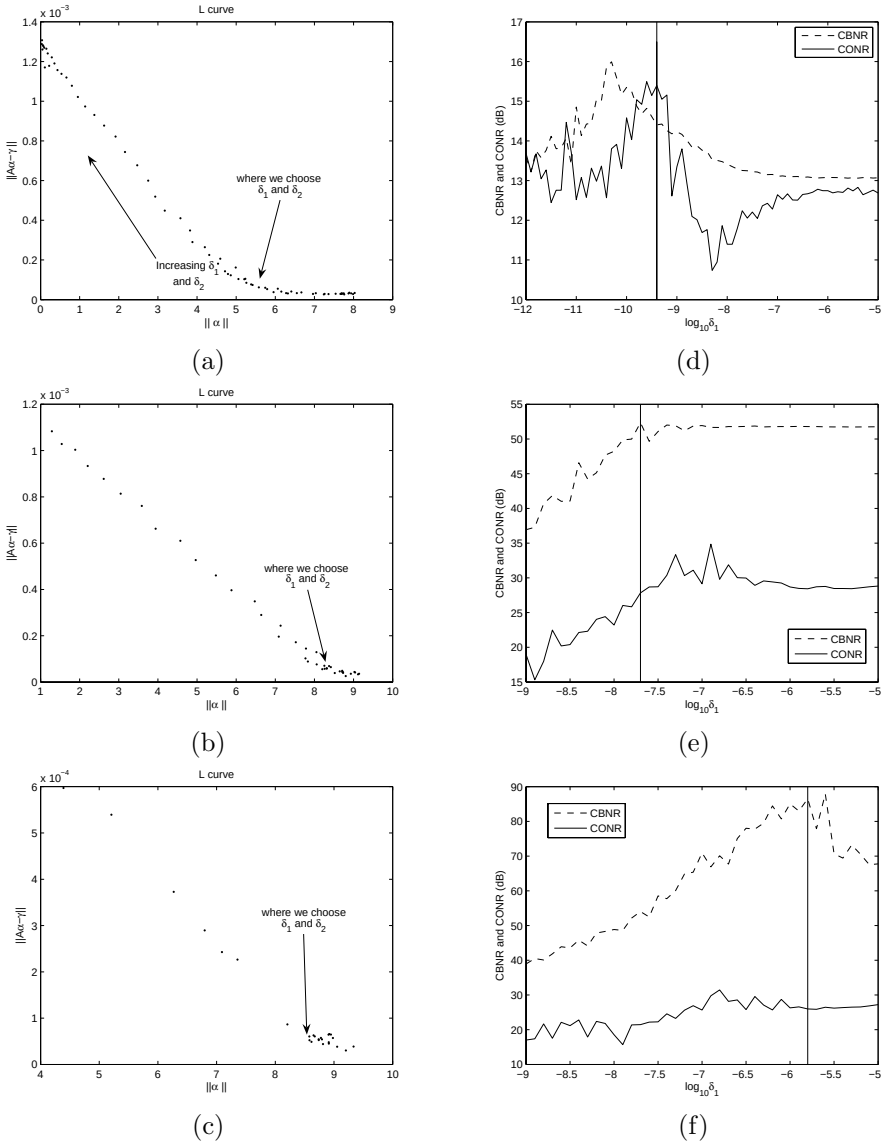

Figure 2. (a) The L-curve of the reconstruction without prior information; (b) The L-curve of the reconstruction with prior information, $\lambda_0 = r_0 = 0.1$; (c) The L-curve of the reconstruction with prior information, $\lambda_0 = r_0 = 0.01$; (d) The CBNR and CONR versus δ_1 in the reconstruction without prior information; (e) The CBNR and CONR versus δ_1 in the reconstruction with prior information, $\lambda_0 = r_0 = 0.1$; (f) The CBNR and CONR versus δ_1 in the reconstruction with prior information, $\lambda_0 = r_0 = 0.01$.

image in the fluorophore region to the standard deviation of the image in the background region. The contrast-to-object noise ratio (CONR) is defined as the ratio of the mean value of the image in the fluorophore region to the standard deviation of the image in the same region.[13]

We plot the CBNR and CONR of the reconstructed image versus δ_1 when $r_0 = \lambda_0 = 1$, $r_0 = \lambda_0 = 0.1$ and $r_0 = \lambda_0 = 0.01$ in the Fig.2 (d), (e) and (f). The solid vertical line indicates the choice of δ_1 from L-curve method. Notice that it always roughly picks out higher values for both CBNR and CONR. Therefore we could conclude that the L-curve method does give comparatively optimal regularization parameters. In Table1, we summarize the CBNR and CONR of the reconstructed image with different choice of r_0 and λ_0, and find significant improvement for both CBNR and CONR of the reconstructed images (the first row in the table is the

reconstruction without prior information).

Table 1. CBNR and CONR when using different r_0 and λ_0 in reconstruction

r_0	λ_0	δ_1	δ_2	CBNR (dB)	CONR (dB)
1	1	4×10^{-10}	8×10^{-11}	14.40	15.40
0.1	0.1	2×10^{-8}	4×10^{-9}	52.34	27.83
0.01	0.01	1.5×10^{-6}	3×10^{-7}	86.50	25.97

4.4 Mismatch of Prior Information

Thus far, the simulations make use of correct and well correlated prior information. In order to see the effects of incorrect prior information, we laterally separated the fluorophore and the region assumed to have fluorophore concentration in prior structural image by 2 cm. The true fluorophore distribution and prior structural image are shown in Fig.3(a) and (b). We set $r_0 = \lambda_0 = 0.1$ and $r_0 = \lambda_0 = 0.01$ and used same method as before to determine δ_1 and δ_2. The reconstructed result is shown in Fig.3 (c) and (d). We find that the true fluorophore concentration is reconstructed in the right position, but greater noise appears at the location of the wrong prior structure. Also, the position of maximum concentration of fluorophore is now located nearer to that region. Although the prior information is completely inconsistent, the reconstructed images has comparable resolution to the result without prior information and is still acceptable.

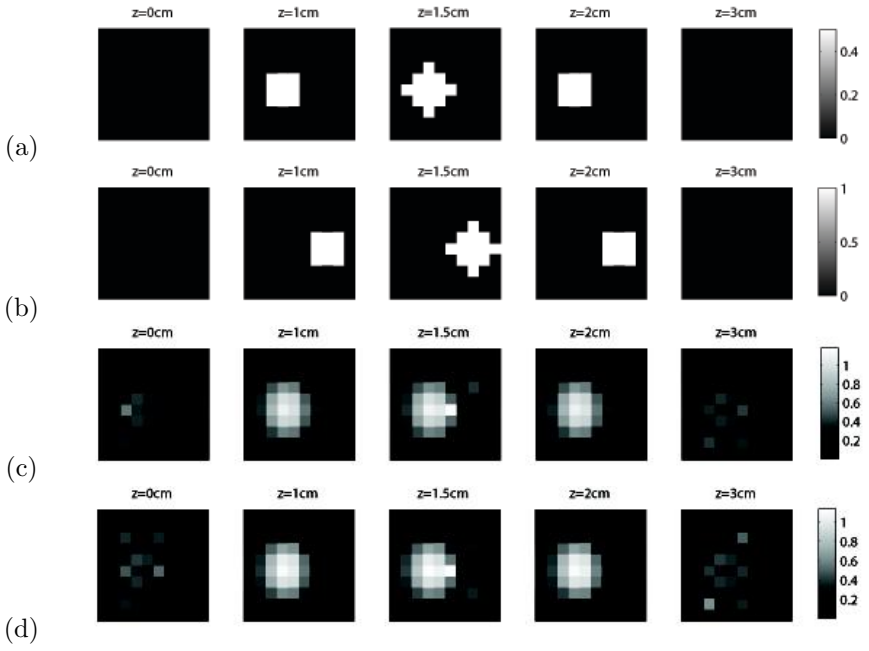

Figure 3. (a) The true image of fluorophore concentration; (b) The wrong prior structural image; (c) Reconstructed image with wrong prior information, $\delta_1 = 1.6 \times 10^{-10}$, $\delta_2 = 3.2 \times 10^{-11}$ and $\lambda_0 = r_0 = 0.1$; (d) Reconstructed image with wrong prior information, $\delta_1 = 1.6 \times 10^{-10}$, $\delta_2 = 3.2 \times 10^{-11}$ and $\lambda_0 = r_0 = 0.01$

5. *IN VIVO* MOUSE EXPERIMENT

5.1 Experiment Configuration

An *in vivo* mouse FMT experiment was also conducted to test our algorithm. The mouse first received intra-tracheal lipopolysaccharide (LPS) instillation to trigger Chronic Obstructive Pulmonary disease (COPD). Next,

a fluorescence probe (Prosense 680, Visen Medical, Woburn MA, excitation 672nm, emission 700-730nm) was instilled into the mouse body. The probe is sensitive to major cathepsin which is associated with inflammation. Based on this animal disease model, the fluorophore is expected to accumulate in the lungs and liver of the mouse.

Optical measurements were obtained on the FMT imaging system developed by Ntziachristos et al.[14] During imaging process, 46 CW light sources were used to generate excitation light and a CCD camera (10^6 pixels) was used to measure the intensity of light on the boundary of imaging domain. The 512×512 pixels of image obtained by the CCD camera was equally divided into 81 square subimages, and the mean value of each subimage was taken as the reading of each detector. The measurements were taken at both excitation and emission wavelength after the instillation of fluorescence probe, and an normalized Born approximation[15] was taken to the data. A slab region of size $3.17 \times 3.17 \times 1.3$ cm indicated by white square box in Fig. 4(a) was meshed into $20 \times 20 \times 9 = 3600$ voxels, and the fluorophore concentration in this region was reconstructed.

For *a priori* anatomical information, MR images were acquired by a 4.7T MRI system (Bruker Instruments, Billerica MA). FMT and MRI imaging was performed sequentially using a rigid frame for animal translation in order to keep the mouse position unchanged. A high resolution MR image slice from the slab region at depth of 0.61 cm is shown in Fig.4(b). The MR images were processed by applying median filter and contrast enhancement before the lungs, other parts of the body and background were segmented and marked. The Fig.4(c) shows the segmentation result at the same depth: the lungs are shown in white, the background in black and other tissue in grey. Based on the animal disease model, it is highly likely that the fluorophore present in the lungs while the background is not expected to contain fluorophore. Notice that although fluorophore was expected to be present in the liver, the prior anatomical information did not account for this.

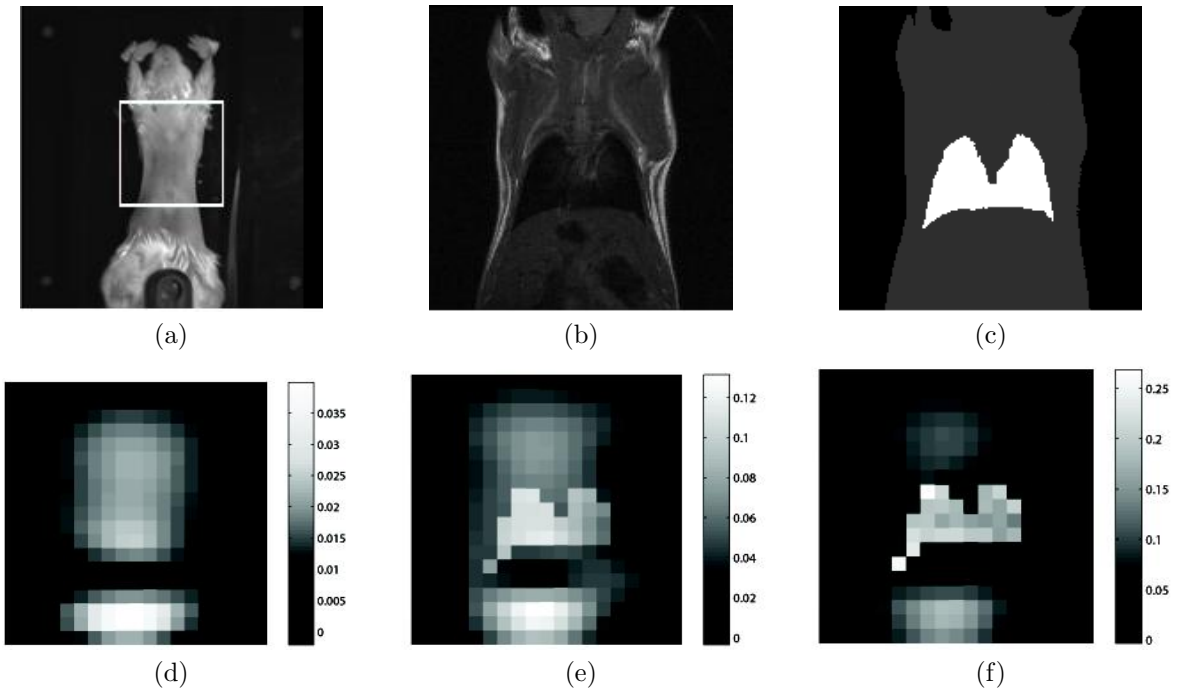

Figure 4. (a) Picture of mouse; (b) The MR image at depth 0.61cm; (c) Segmented MR image at depth 0.61cm; (d) Reconstructed image without prior information, $\delta_1 = 10^6$ and $\delta_2 = 2.3 \times 10^5$; (e) Reconstructed image with prior information, $r_0 = \lambda_0 = 0.5$, $r_1 = 0.8$, $\delta_1 = 10^6$ and $\delta_2 = 2.1 \times 10^5$; (f) Reconstructed image with prior information, $r_0 = \lambda_0 = 0.1$, $r_1 = 0.5$, $\delta_1 = 10^6$ and $\delta_2 = 1.8 \times 10^5$.

5.2 Reconstruction Result

First, we reconstructed the image using traditional Tikhonov regularization without prior anatomical information. The optimal regularization parameters were chosen according to the L-curve. The result is shown in Fig.4(d).

Next, the prior information was used in reconstruction. The prior anatomical images contained three different regions and two boundaries. We assigned a different penalty on the magnitudes of voxels in three regions and identical values to the last eigenvalues of $\tilde{B}(\mathbf{x})$ for voxels on two boundaries:

$$r_{m,n} = \begin{cases} r_0 & \text{when } m = n \text{ and } i\text{th voxel is in lungs,} \\ r_1 & \text{when } m = n \text{ and } i\text{th voxel is in other parts of mouse body,} \\ 1 & \text{when } m = n \text{ and } i\text{th voxel is in background,} \\ 0 & \text{when } m \neq n, \end{cases}$$

$$\lambda_j^{(i)} = \begin{cases} \lambda_0 & j = 3 \text{ and } i\text{th voxel is on the boundary between any two regions,} \\ 1 & \text{otherwise.} \end{cases}$$

Based on our animal disease model, $0 < r_0 < r_1 < 1$ and $0 < \lambda_0 < 1$. To avoid hard constraint during the reconstruction, we chose moderate values $r_0 = \lambda_0 = 0.5$, $r_1 = 0.8$ and $r_0 = \lambda_0 = 0.1$, $r_1 = 0.5$. δ_1 and δ_2 were also determined by L-curve method as before. The reconstructed images are shown in Fig.4(e) and (f) respectively.

The result without using prior information shows two major regions of fluorophore concentration: the bigger region diffuses through upper half of the mouse's body and the smaller region with a higher value is located around the liver. When using prior anatomical information in reconstruction, the major fluorophore concentration is reconstructed within the lungs region. In the same time, the fluorophore concentration in liver is also captured, although it is not contained in prior anatomical information. The result is consistent with our animal disease model, and significant improvement of resolution and contrast is achieved by using prior information. Notice that when smaller values of r_0, r_1 and λ_0 are chosen, the sharper boundaries between different regions show in the reconstructed image and the result may be biased. Therefore, the value of these parameters should be chosen carefully, and visual result may need to be checked when necessary.

6. CONCLUSION

We incorporated prior anatomical information into generalized Tikhonov regularization by using two penalty terms, first introduced by Arridge and Kaipio. The L-curve method was used to determine optimal regularization parameters in reconstruction. We determined that when the prior information is consistent with true fluorophore concentration, the resolution and contrast of reconstructed images was improved significantly both in the simulation study and in the *in vivo* mouse experiment. Incorrect prior information does not strongly bias errors in the reconstruction, although the result is not improved at all. These results show us the prospect of using prior information to guide the reconstruction of FMT.

A possible future exploration of how the parameters inside the two penalty terms $R(\alpha)$ and $B(\alpha)$ can affect the reconstruction result and the optimal methodology of choosing these parameters may prove fruitful. For this work, we only consider the regularization within a deterministic framework. Thus, more work may need to be done to incorporate *a priori* information in hierarchical Bayesian framework in which the correlation between fluorophore distribution and anatomical image could be explored further.

REFERENCES

1. V. Ntziachristos, J. Ripoll, L. V. Wang, and R. Weissleder, "Looking and listening to light: the evolution of whole-body photonic imaging," *Nature Biotechnology* **23**, pp. 313–320, 2005.
2. Y. Lin, H. Gao, O. Nalcioglu, and G. Gulsen, "Fluorescence diffuse optical tomography with functional and anatomical a priori information: feasibility study," *Phys. Med. Biol* **52**, pp. 5569–5585, 2007.
3. S. C. Davis, H. Dehghani, J. Wang, S. Jiang, B. W. Pogue, and K. D. Paulsen, "Image-guided diffuse optical fluorescence tomography implemented with laplacian-type regularization," *Optics Express* **15**, pp. 4066–4082, 2007.
4. B. Brooksby, S. Jiang, H. Dehghani, B. W. Pogue, K. D. Paulsen, J. Weaver, C. Kogel, and S. P. Poplack, "Combining near-infrared tomography and magnetic resonance imaging to study in vivo breast tissue: implementation of a laplacian-type regularization to incorporate magnetic resonance structure," *J. Biomedical Optics* **10**, pp. 051504 1–10, 2005.

5. M. Guven, B. Yazici, X. Intes, and B. Chance, "Diffuse optical tomography with a priori anatomical information," *Physics in Medicine and Biology* **50**, pp. 2837–2858, 2005.
6. G. Boverman, E. L. Miller, A. Li, Q. Zhang, T. Chaves, D. H. Brooks, and D. A. Boas, "Quantitative spectroscopic diffuse optical tomography of the breast guided by imperfect a priori structural information," *Physics in Medicine and Biology* **50**, pp. 3941–3956, 2005.
7. M. Guven, B. Yazici, and V. Ntziachristos, "Fluorescence optical tomography with a priori information," *Multimodal Biomedical Imaging II* **6431**(1), p. 643107, SPIE, 2007.
8. S. R. Arridge, "Optical tomography in medical imaging," *Inverse Problem* **15**, pp. R41–R93, 1999.
9. M. S. Patterson and B. W. Pogue, "Mathematical model for time-resolved and frequency-domain fluorescence spectroscopy in biological tissues," *Appl. Opt.* **30**, pp. 1963–1974, 1994.
10. S. R. Arridge and M. Schweiger, "Inverse methods for optical tomography," in *IPMI '93: Proceedings of the 13th International Conference on Information Processing in Medical Imaging*, pp. 259–277, Springer-Verlag, (London, UK), 1993.
11. J. P. Kaipio, V. Kolehmainen, M. Vauhkonen, and E. Somersalo, "Inverse problem with structural prior information," *Inverse Problem* **15**, pp. 713–729, 1999.
12. P. C. Hansen, *Rank-Deficient and Discrete Ill-Posed Problems: Numerical Aspects of Linear Inversion*, SIAM Press, Philadelphia, PA, 1998.
13. A. Li, E. L. Miller, M. E. Kilmer, T. J. Brukilacchio, T. Chaves, J. Stott, Q. Zhang, T. Wu, M. Chorlton, R. H. Moore, D. B. Kopans, and D. A. Boas, "Tomographic optical breast imaging guided by three-dimensional mammography," *Applied Optics* **42**, pp. 5181–5190, 2003.
14. E. E. Graves, J. Ripoll, R. Weissleder, and V. Ntziachristos, "A submillimeter resolution fluorescence molecular imaging system for small animal imaging," *Med. Phys.* **30**, pp. 901–911, 2003.
15. V. Ntziachristos and R. Weissleder, "Experimental three-dimensional fluorescence reconstruction of diffuse media by use of a normalized born approximation," *Optics Letters* **26**, pp. 893–895, 2001.